



ADVANCES IN THE PREDICTION OF PISTON TOP RING FRICTIONAL BEHAVIOUR

A. SENATORE, V. D'AGOSTINO

UNIVERSITY OF SALERNO, DEPARTMENT OF MECHANICAL ENGINEERING,
FISCIANO (SA), ITALY

ABSTRACT:

This paper presents the results of simulations on the energy loss for the friction interaction top ring/cylinder wall in a SI engine taking into account the mixed lubrication (ML) regime and considering different engine operating conditions, lubricant viscosity, surface roughness. The oil film thickness prediction describes a sensible different behavior in the case of the entire stroke in ML regime while the plots confirm bigger portions of the four strokes in hydrodynamic regime for high speed/low load operating conditions. A quite insensible response of the friction coefficient is observed for ring roughness around $1.00 \mu\text{m}$, while an effective gain on the mechanical efficiency is achievable only below $0.40 \mu\text{m}$.

KEYWORDS:

simulation, engine mechanical efficiency, friction losses, mixed lubrication

1. BRIEF LITERATURE REVIEW

A significant share of the total fuel energy (Figure 1) in a modern automotive engine is dissipated in the friction upper compression ring/cylinder wall friction. On this basis, the lubrication of the piston ring has been an important research matter for many years because it is extensively accepted that the interaction at the ring-cylinder wall interface provides substantial effects on friction, wear, oil consumption and power loss in ICEs, as showed in the papers of Furuhama et. al. [1], Taylor [2] and Takiguchi et al. [3].

The piston rings are basically a set of sliding seals whose purpose is to separate the combustion gases above the piston from the crankcase environment below. The most common arrangement is a set of three rings (Figure 2), the upper compression ring, the lower compression ring and the oil control ring.

The ring-cylinder wall interface is particularly interesting as it has been estimated to account for 20% of the total engine mechanical friction by Ting [4], due to the most severe environment in terms of temperature and load, so much effort has been directed to this particular ring. Because of the piston is during its stroke always in an unsteady state, the frictional behaviour of the rings is very complex.

This paper introduces the results of simulations concerning the friction interaction top ring/cylinder wall of a SI engine, taking into account the mixed lubrication (ML) regime and considering different engine operating conditions, lubricant viscosity, surface roughness.

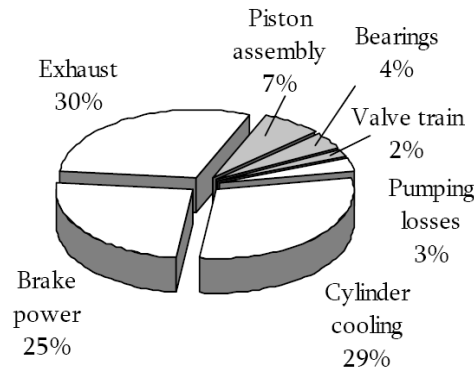


Figure 1: Fuel energy in an internal combustion engine (friction losses in grey, 4 krpm, full load)

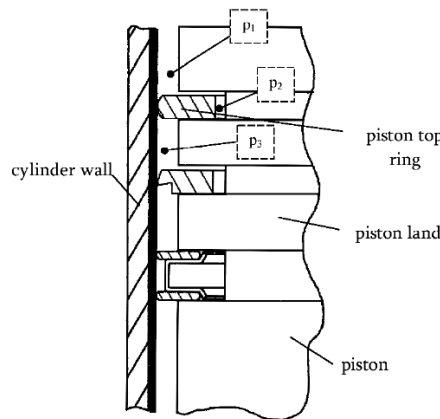


Figure 2: Geometry of the lubricated pair piston rings-cylinder wall

2. THE MIXED LUBRICATION REGIME FOR THE RING

The implemented mathematical model is based on the sharing of the total load acting in the ring radial direction between the hydrodynamic lubrication (HDL) force and the solid-to-solid interactions along the asperities of the surfaces as approached by Greenwood et al. [5], Gelinck et al. [6] and Senatore et al. [7]:

$$F_R = F_C + F_H \quad (1)$$

with F_C the load carried by the interacting asperities and F_H the one carried by the hydrodynamic component. The total friction force F_f , acting on the ring in tangential direction, is the sum of the friction force between the asperities and the shear force about the HDL regime:

$$F_f = \sum_{i=1}^{N_a} \iint_{A_{C_i}} \tau_{C_i} dA_{C_i} + \iint_{A_H} \tau_H dA_H \quad (2)$$

with N_a the number of asperities in contact, A_{C_i} the area of contact of a single asperity i ; τ_{C_i} the shear stress at the asperity contact i ; A_H the contact area of the ring in HDL regime and τ_H the shear stress of this component.

The friction coefficient f can be calculated by the following equation:

$$f = \frac{F_f}{F_R} = \frac{F_{f,b} + F_{f,h}}{F_R} = \frac{\sum_{i=1}^{N_a} \iint_{A_{C_i}} \tau_{C_i} dA_{C_i} + \iint_{A_H} \tau_H dA_H}{F_R} \quad (3)$$

Both the components, F_C and F_H , show a strongly dependence by the height h_0 of the central point of the piston top ring (barrel shape), i.e., the minimum nominal distance between the ring and the cylinder wall.

2.1. The friction due to the deformation of the asperities

For the direct contact between the surfaces the pressure generated by the deformation of the asperities is taken into account according to [6]:

$$p_c(x) = \frac{2}{3} n \beta \sigma_s \sqrt{\frac{\sigma_s E'}{\beta}} F_{3/2} \left(\frac{h(x)}{\sigma_s} \right) \quad (4)$$

with $h(x)$ the separation between the two surfaces, n the density of the asperities, β the average radius of the asperities and σ_s the standard deviation of the height distribution of the summits.

The function $F_{3/2}$ is given by the following expression:

$$F_{3/2}(h) = \int_h^{\infty} (s-h)^{3/2} \phi(s) ds \quad (5)$$

where, the ϕ function is the standardized height distribution of the summits, assumed given by the Gaussian distribution law (6a); the (6b) allows calculating the radial asperity force:

$$\phi(s) = \frac{1}{\sqrt{2\pi}} \text{Exp} \left(-\frac{1}{2} s^2 \right) \quad (6a)$$

$$F_b = \int_0^B \int_0^L p_c(x) dA \quad (6b)$$

2.2. The hydrodynamic lubrication model

The normal load due to the HDL regime and the shear stress due to the film lubricant have been calculated by integrating the Reynolds equation in the one-dimensional form:

$$\frac{\partial}{\partial x} \left(h^3 \frac{\partial p}{\partial x} \right) = 6\mu U \frac{\partial h}{\partial x} + 12\mu \frac{\partial h}{\partial t} \quad (7)$$

with the boundary conditions as in [8], with the data about the areas at p_1 , p_2 and p_3 (Figure 2), from [9].

The viscous shear stress is described by:

$$\tau_H(x) = -\mu \frac{U}{h(x)} + \frac{h(x)}{2} \frac{dp}{dx} \quad (8)$$

In this research, the lateral drag motion of the entire piston ring due to the approaching secondary-motion of the piston to the cylinder wall has not been considered, while other analysis take into account this phenomenon to analyze the ring flexibility as in D'Agostino et al. [10]. Then the ring distance from the cylinder is evaluated with the axial symmetry assumption and in a quasi-static evolution.

3. SIMULATION ALGORITHM

The data of the Table 1 have been involved in all the simulations about the analysis of the friction behaviour of the considered piston ring. The implemented algorithm calculates the monotonically decreasing function F_c versus h_0 with the chosen set of geometrical and material resistance data.

Then, for the instantaneous values of the piston speed (U) and the pressure boundary conditions, the Reynolds equation is solved allowing the numerical iterations for the inversion of the (9), in the unknown variable h_0 :

$$F_c(h_0) + F_H(h_0, U, p_1, p_3) - F_{R,t} - F_{R,g}(p_2) = 0 \quad (9)$$

At each step of the numerical procedure, the crankshaft position θ is increased by a defined step (0.010 rad), the U value is updated as well as the pressure

conditions from the indicated cycle; then, iterations are performed on the HDL and asperities components for satisfying the equilibrium condition with the algebraic constrain given by the total radial load F_R , i.e., the sum of the ring tension and the gas pressure acting on the ring back side (9).

The numerical simulations were carried out with the inter-ring gas pressures (see Figure 2) according to [9] and the data in Table 1.

Once the previous equation has solved and the minimum ring distance from the cylinder wall h_0 is known, the friction forces and the friction coefficient can be calculated using the relationships above described (2, 3 and 8).

TABLE 1. SI engine, displacement per cylinder: 311 cm³

Parameter	Symbol	Value	Unit
Density of asperities	n	10^{11}	m ⁻²
Average radius of asperities	β	10	μm
Standard deviation of the asperities	σ_s	$0.20 \div 0.60 \div 1.00^*$	μm
Reduced modulus of elasticity	E'	231	GPa
Length of the top ring	L_1	1.50	mm
Cylinder bore	B	76.0	mm
Oil viscosity	μ	$5.0 \div 15.0^* \div 25.0$	mPa s
Maximum pressure of the indicated cycle	p_{cyl}	$0 \div 10 \div 30$	bar
Engine speed	N	1000, 3000, 5000	rpm
Connecting-rod length	L_{CR}	129	mm
Characteristic ratio of the slider-crank mech.	L_{CR} / R_c	3.30	-

* Standard condition unless otherwise specified

4. RESULTS AND DISCUSSION

4.1. Effect of the radial load

The Figures 3 compare the predicted effects of the radial load to the piston ring on the friction coefficient for an engine speed equal to 3000 rpm.

The plots are presented with the choice of the oil dynamic viscosity as parameter. In an actual engine model, this radial force is the sum of the ring tension and the gas pressure acting in the radial direction (chamber at pressure p_2).

Two effects can be observed as immediate upshot:

- 1) for increasing radial load acting on the back side of the ring due to a bigger pressure in the cylinder, the transition to fully developed HDL regime is delayed during the expansion after the TDC position ($\theta = 2 \pi$); this transition occurs at an early crankshaft position θ for the lubricant with viscosity 25 mPa s;
- 2) the whole four strokes exhibit interaction in mixed-lubrication conditions for oil viscosity equal to 5 mPa s.

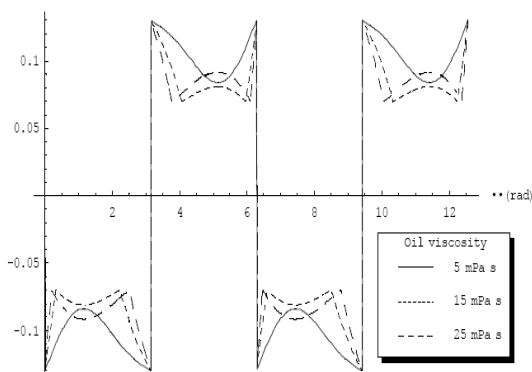


Figure 3(a): Friction coefficient at 3000 rpm, open valves

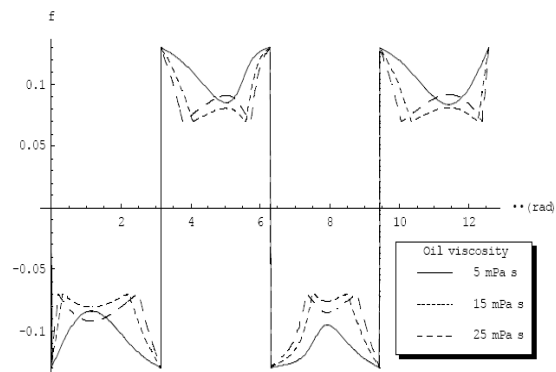


Figure 3(b): Friction coefficient at 3000 rpm, $p_{\text{cyl}} = 30 \text{ bar}$

4.2. Effect of the speed

The lubricant film thickness and the load carried by oil pressure increase with increasing running speeds. For this reason, when the engine runs at low speed the existence of high friction coefficients near dead centres, indicating metal-to-metal contact, is extended to a big portion or the entire piston stroke. The Figures 4 and 5 show that for engine speed equal to 3000 and 5000 rpm, the transition to fully developed HDL regime occurs in the first 10% of the stroke path, while a considerable first fraction of the expansion stroke shows evidence of the coexistence of boundary and hydrodynamic lubrication, due to the increased cycle pressure and, then, radial ring load.

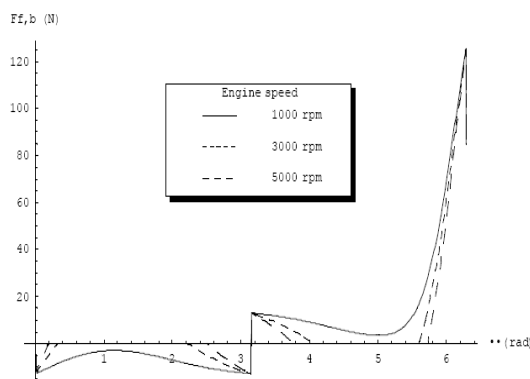


Figure 4: Boundary friction force
($p_{cyl} = 30 \text{ bar}$, $\mu = 15 \text{ mPa s}$)

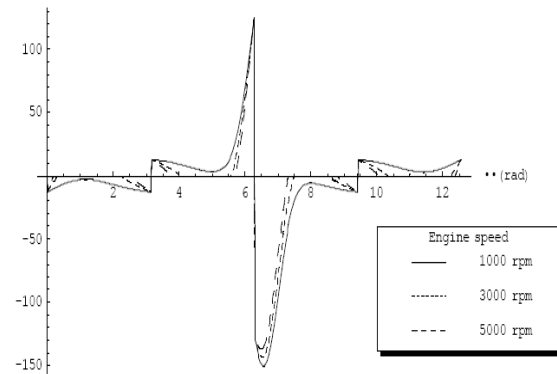


Figure 5: Boundary friction force
($p_{cyl} = 30 \text{ bar}$, $\mu = 15 \text{ mPa s}$)

As predictable, the higher is the viscosity and the higher the HDL friction force Figure 6(a), while the oil film thickness demonstrates a sensible different behaviour in the case of the entire stroke in mixed lubrication regime, Figure 6(b).

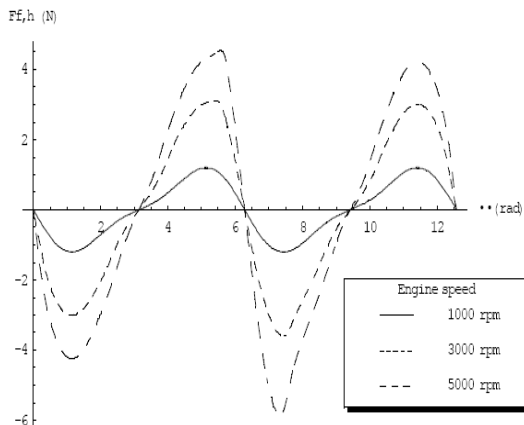


Figure 6: (a) Hydrodynamic friction force
($p_{cyl} = 30 \text{ bar}$, $\mu = 15 \text{ mPa s}$)

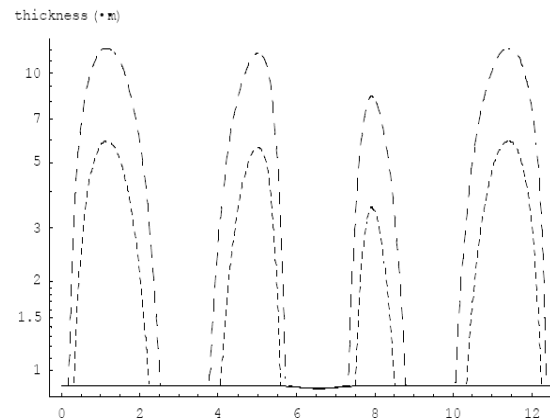


Figure 6: (b) Oil film thickness
($p_{cyl} = 30 \text{ bar}$, $\mu = 15 \text{ mPa s}$)

The following two figures illustrate on each plot the HDL friction force in coexistence with the boundary one (dash line) and the part of stroke where the oil film is fully developed (solid line).

The figures confirm bigger portion of stroke in HDL regime for high speed/low load operating conditions.

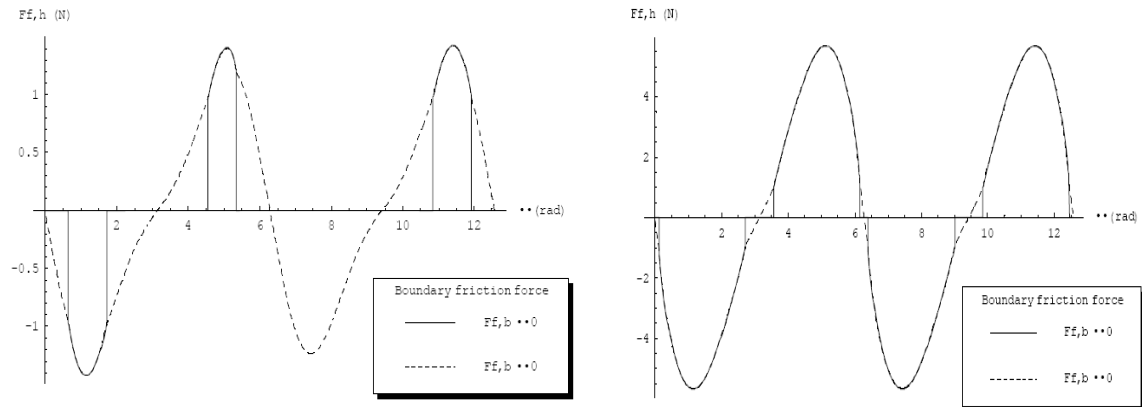


Figure 7: Hydrodynamic friction force in ML-regime (dash line) and HDL-regime (solid line) at 1000 rpm; (a) $p_{cyl} = 30$ bar; (b) open valves

4.3. Effect of the surface roughness

This analysis on the ML-regime for the piston top confirms a quite insensible behaviour of the friction coefficient for ring roughness in the range $0.60 \div 1.00 \mu\text{m}$, while an effective gain on the mechanical efficiency is achievable in the range $0.20 \div 0.40 \mu\text{m}$. This outcome may lead the designers toward a balanced cost-benefit analysis. The Figure 8 proves the significant impact of the surface roughness, in the above mentioned ranges.

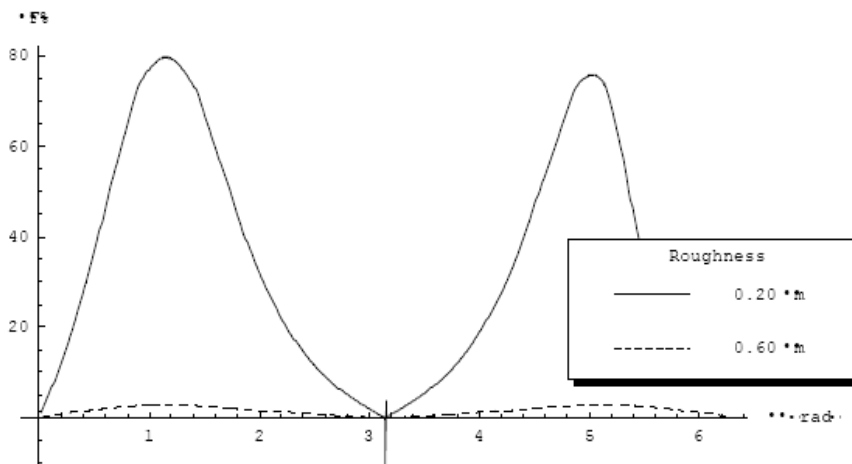


Figure 8: Boundary friction force decreasing (abs. value) at 1000 rpm and $p_{cyl} = 30$ bar; roughness standard value $\sigma_s = 1.00 \mu\text{m}$

4.4. Effect of the oil viscosity

The analysis takes into account the lubricant viscosity in the range $5.0 \div 25.0$ mPa s, the typical values for the commercial defined 0W30 or 5W30 along the temperature range $70 \div 100^\circ\text{C}$. For higher viscosity, the lubrication regime is hydrodynamic over most of the stroke, also in presence of the high radial load during the expansion stroke, as shown in the Figure 9, where the boundary friction force declines to zero with the delay of the transition boundary-hydrodynamic regime for the lower viscosity oil up to 80 crankshaft degrees.

The four figures in Figure 10 illustrate the effect of the viscosity on the total friction force acting on the ring at 1000 and 5000 rpm, for a maximum cycle pressure equal to 10 and 30 bar, while the surface roughness is $1.00 \mu\text{m}$ in all the cases.

The oil with low viscosity exhibits lower friction force for high speed and low radial load, while the high viscosity has better effect on the mechanical efficiency on the opposite side.

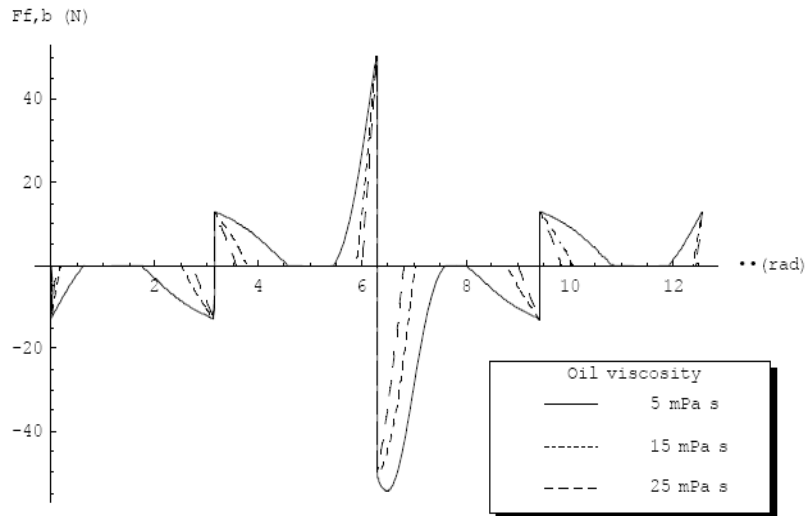


Figure 9: Boundary friction force at 5000 rpm, $p_{cyl} = 10$ bar

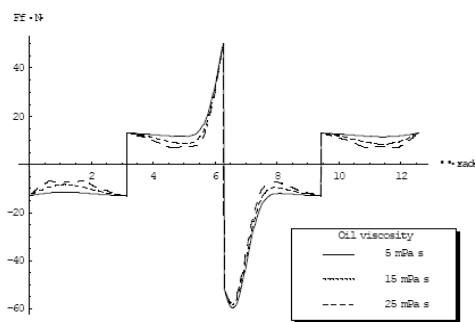


Figure 10(a): Total friction force;
1000 rpm, $p_{cyl} = 10$ bar

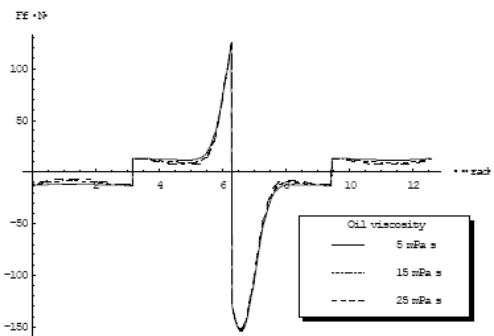


Figure 10(b): Total friction force;
1000 rpm, $p_{cyl} = 30$ bar

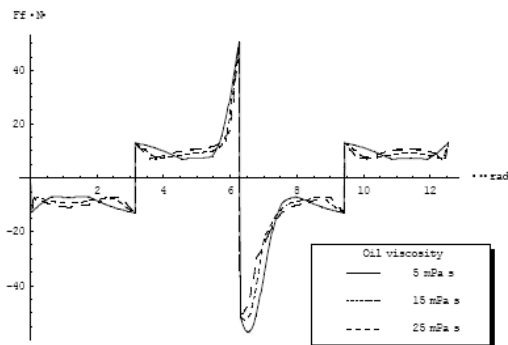


Figure 10(c): Total friction force;
5000 rpm, $p_{cyl} = 10$ bar

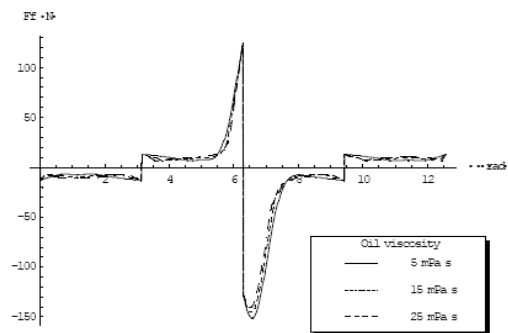


Figure 10(d): Total friction force;
5000 rpm, $p_{cyl} = 30$ bar

Another way to get assessments about the viscosity inference on the friction engine dissipation is the comparison among the instantaneous friction power loss.

As underlined by the following figure, the operating condition with high engine speed (5000 rpm) and no-load (open valves) is the limit one when the oil with the minimum viscosity has to be preferred. The figure 12 shows a good behaviour of the other two lubricants for increasing radial loads.

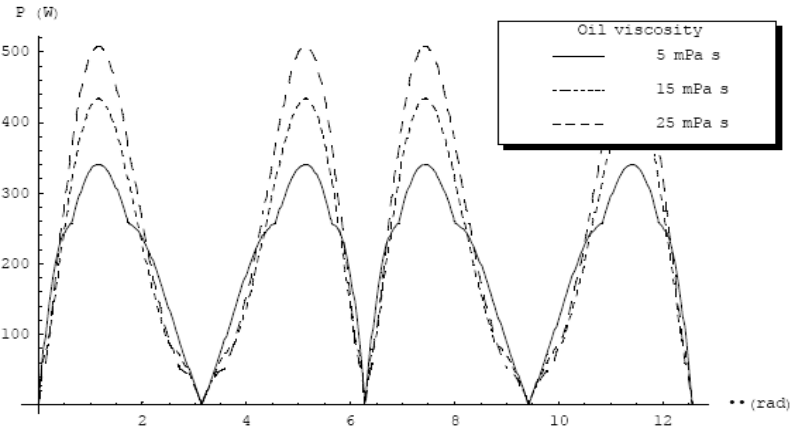


Figure 11: Power loss at top piston ring at 5000 rpm, no load ($p_{cyl} = 0$)

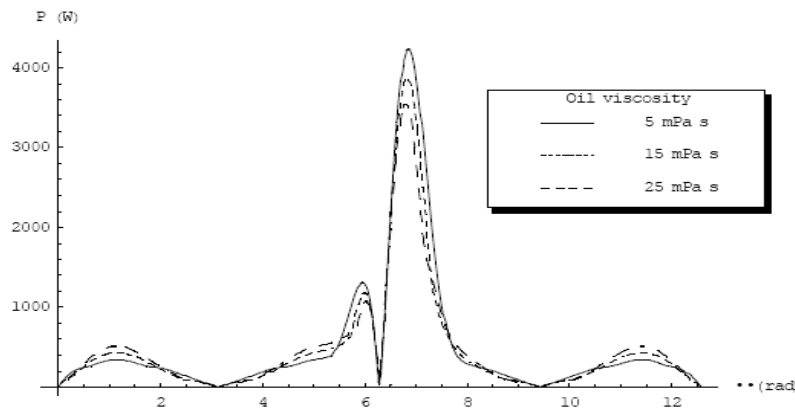


Figure 12: Power loss at top piston ring at 5000 rpm, $p_{cyl} = 30$ bar

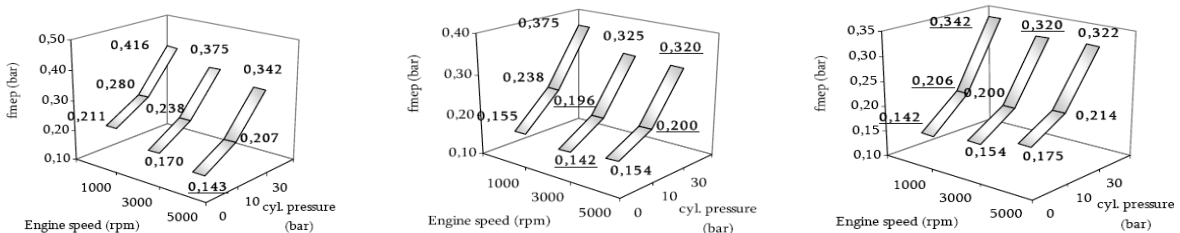
The following plots introduce the friction work in a whole thermodynamic cycle (4π rad) expressed in the conventional terms of friction mean effective pressure, work divide by the displacement, covering the operating conditions proposed above:

- low/medium/high speed: 1000, 3000, 5000 rpm;
- low/medium/high load: cylinder pressure (indicated cycle): 0 bar (open valves), 10 bar (motoring), 30 bar (medium/full load).

$$W_f = \int_{s=0}^{s=8R_c} F_f(s) ds = \int_0^{4\pi} F_f(\theta) \frac{U(\theta)}{\omega(\theta)} d\theta \quad (10)$$

$$fmep = \frac{W_f}{V} = \frac{1}{\pi R^2 (2R_c)} \int_0^{4\pi} F_f(\theta) \frac{U(\theta)}{\omega(\theta)} d\theta \quad (11)$$

The underlined numbers in the Figure 13 identify the lower $fmep$ value for the specified load/speed combination.



Figures 13: Friction mean effective pressure, $fmep$ (bar) oil viscosity
 (a) 5.0 mPa s; (b) 15.0 mPa s; (c) 25.0 mPa s

5. CONCLUDING REMARKS

The results of simulations about the friction interaction of the piston upper compression ring of a SI automotive engine taking into account the mixed lubrication regime have been presented.

Lower oil viscosity allows lower friction force for high speed and moderate radial load, while the high viscosity one produces better effect on the mechanical efficiency on the opposite side. This analysis reveals a quite insensible behaviour of the friction coefficient for ring roughness in a wide range in the neighbour of $1.00 \mu\text{m}$, while an effective gain on the mechanical efficiency is achievable only declining to the range $0.20\div 0.40 \mu\text{m}$.

The oil film thickness prediction describes a sensible different behaviour in the case of the entire stroke in mixed lubrication regime.

The plots confirm bigger portion of the four strokes in HDL regime for high speed/low load operating conditions. The outcomes show that for engine speed up to 3000 rpm, the transition to fully developed HDL regime occurs in the first 10% of the stroke, while a considerable first fraction of the expansion stroke shows evidence of the coexistence of boundary and hydrodynamic lubrication due to the increased cycle pressure and, then, radial ring load.

The good agreement with the theoretical and experimental results of [9] and [11], allows using this mathematical approach/numerical procedure as an effective tool for predicting the piston rings friction losses in a wide range of engine operating conditions and rings arrangement.

List of symbols

A_{ci}	Area of single asperity contact	p	Hydrodynamic pressure
A_H	Contact area of the hydrodynamic component	p_c	Asperities local contact pressure
B	Cylinder bore	p_{cyl}	Gas pressure from indicated cycle
E'	Reduced modulus of elasticity	p_i	Pressure in the areas of Fig. 2
F_C	Normal load carried by the asperities	R	Piston radius
F_H	Normal load carried by hydrodynamic comp.	R_C	Crankshaft radius
F_f	Ring friction force	U	Piston axial speed
F_R	Total normal load	V	Engine displacement per cylinder
$F_{R,t}$	Ring tension	x	Ring/Piston axial coordinate
$F_{R,g}$	Radial force due to the gas pressure p_2	t	Time
$F_{3/2}$	Asperities height function	β	Average asperities radius
h	Oil film thickness	ϕ	Standardized height distribution
h_0	Minimum ring distance from cylinder wall	μ	Oil dynamic viscosity
L_{CR}	Connecting-rod length	σ_s	Height distribution standard deviation
n	Density of asperities	τ_{ci}	Shear stress at the asperity contact
N	Engine speed (rpm)	τ_H	Shear stress of the hydrodynamic lubrication
N_a	Number of contact asperities	ω	Engine speed (rad s^{-1})

REFERENCES

- [1.] FURUHAMA, S., TAKIGUCHI, M. (1979). *Measurement of piston frictional force in actual operating diesel engine*, SAE Paper No. 790855.
- [2.] TAYLOR C. M. (1992). *Fluid-Film Lubrication in the Internal Combustion Engines: an Invited Review*, J. Phys. D: Appl. Phys., Vol. 25.
- [3.] TAKIGUCHI, M., MACHIDA, K., FURUHAMA, S. (1988). *Piston friction force of a small high speed gasoline engine*, J. of Tribology, ASME. Vol. 110(1): pp.112-118.
- [4.] TING, L.L. (1985). *A review of present information on piston ring tribology*, SAE paper no. 852355.
- [5.] GREENWOOD, J.A., WILLIAMSON, J.B.P. (1966). *Contact of nominally flat surfaces*, Phil. Trans. R. Soc. London, Series A, Vol.19, pp.295-300.

- [6.] GELINCK, E.R.M., SCHIPPER, D.J. (2000). *Calculation of Stribeck curves for line contacts*, Tribology Int., Vol. 33, pp. 175-181.
- [7.] SENATORE, A., CIORTAN, S. (2004). *Oil ring friction loss simulation considering the mixed lubrication regime*, Proc. of VAREHD 12, Int. Conf.
- [8.] D'AGOSTINO, V., DELLA VALLE, S., RUGGIERO, A., SENATORE A. (2005). *On the effective length of the top piston ring involved in hydrodynamic lubrication*, Lubrication Science, Leaf Coppin – Vol. 17-3 (17) 309 ISSN 0954-0075, pp. 309-318.
- [9.] YUN, J. E., CHUNG, Y., CHUN, S. M., LEE, K. Y. (1995). *An application of simplified average Reynolds equation for mixed lubrication analysis of piston ring assembly in an internal combustion engine*, SAE paper no. 952562. SAE.
- [10.] D'AGOSTINO, V., SENATORE, A. (2005). *Piston ring behaviour simulation considering mixed-lubrication and flexibility*, Proc. of International Design Engineering Technical Conferences & Computers and Information in Engineering Conference - IDECT/CIE, ASME Conference.
- [11.] AKALIN, O., NEWAZ, G.M. (2001) *Piston ring-cylinder bore friction modelling in mixed lubrication regime: Part II – Correlation with bench test data*, ASME J. of Tribology, Vol.123, pp. 219-223, 2001.